Single-piston quantum engine

A. Rodin *

Yale-NUS College, 16 College Avenue West, Singapore 138527, Singapore;
Centre for Advanced 2D Materials, National University of Singapore, Singapore 117546, Singapore;
and Department of Materials Science and Engineering, National University of Singapore, Singapore 117575, Singapore

(Received 13 March 2024; accepted 1 May 2024; published 16 May 2024)

A single-piston quantum engine based on a harmonic oscillator acting as the working fluid is proposed. Using the fact that the interaction between the piston and the oscillator depends on the extent of the oscillator wave function, one can control this interaction by modifying the oscillator temperature. By retracting the piston when the interaction is weak (hot oscillator) and returning it to the original position when the coupling is strong (cold oscillator), useful work can be performed assuming the interaction is attractive. The cycle of the engine is simulated numerically using two different powering protocols: bath and measurement. Using the collision model for the baths, the engine is shown to reach a steady state with positive work output.

DOI: 10.1103/PhysRevResearch.6.023174

I. INTRODUCTION

The purpose of an engine is to convert energy into work while operating cyclically. Although essentially all commonplace implementations are rooted in classical physics for their operation, there is a growing interest in quantum engines [1,2]. Unlike their classical analogs, where the working fluid is typically a liquid or a gas, quantum engines employ quantum components. Some examples of these quantum working fluids are two-level systems [3–6], single [7–18] or multiple [19,20] harmonic oscillators, or photons [21,22]. Another feature that sets quantum and classical varieties apart is how they are powered. Classical implementations rely on hot reservoirs as energy sources and require cold baths to expel waste heat. Quantum versions, on the other hand, can also obtain the required energy from measurements [23–32], which act as effective hot baths.

When discussing quantum engines, one generally assumes that there is a way to transfer the work released during the power stroke of the cycle to some piston without explicitly focusing on this engine component. A recent work [22] addressed the problem of energy transfer by describing an engine that uses modes in an optical cavity as the working fluid. In the proposed engine, one of the cavity walls is mobile and acts as a piston, allowing the fluid to compress and expand. The fluid, in turn, exerts radiation pressure on the mobile piston, transferring energy to it. The engine is powered by heat baths coupled to the working fluid in an alternating fashion, as is typical for heat engines. Because the frequency of the optical modes is inversely related to the cavity length, the proposed configuration is an elegant implementation of the prototypical quantum heat engine which uses a harmonic oscillator as the working fluid and relies on the variation of the oscillator frequency in the course of operation.

Introduced in this paper is another implementation of a quantum engine in which the piston plays an integral role. Even though the working fluid employed here is the commonly used harmonic oscillator, the operation principle fundamentally differs from the approaches that draw their inspiration from the classical analogs. This engine does not rely on expansion and compression of the working fluid, setting it apart from the previously studied systems, including Ref. [22]. Instead, the engine uses the fact that it is possible to modify the coupling strength between quantum engine components by controlling their energies [33].

The proposed cycle is shown in Fig. 1. The system consists of a harmonic oscillator acting as the working fluid and a moving piston. The two components are coupled via an attractive interaction. The cycle starts with the oscillator in a low-energy state and the piston positioned close to the equilibrium point of the oscillator. As the first step, the energy of the oscillator is increased by adding heat. This heating increases the extent of the oscillator wave function, reducing the interaction strength between the oscillator and the piston. The weakened interaction allows the piston to be retracted from the oscillator in the second step of the cycle with a reduced energy cost. With the piston retracted, the oscillator is cooled down using a cold bath, reducing the extent of its probability distribution. Finally, the piston returns to its initial position. Due to the enhanced interaction because of the narrower oscillator wave function in the final step, more work is released during this phase than was required for retraction, resulting in a net-positive work output.

As mentioned above, the heat required for quantum engine operation can originate either from heat baths or measurements. Therefore, after introducing the general model for the

*alerodin@gmail.com

engine in Sec. II, two prototypical approaches using a hot bath and measurements are demonstrated in Sec. III. The summary of this paper as well as the discussion regarding the experimental implementation are given in Sec. IV.

All computations are performed using JULIA [34]. The plots are made using the Makie.jl package [35] using the color scheme designed for colorblind readers [36]. The scripts used for computing and plotting can be found at Ref. [37].

II. MODEL

A. Oscillator-piston interaction

The time-dependent Hamiltonian for an isolated oscillator-piston system, expressed in terms of the oscillator energy $\hbar\Omega$, is given by

$$\hat{H}(\tau) = \left(\hat{a}^\dagger \hat{a} + \tfrac{1}{2}\right) + \Phi[\hat{x}, y(\tau)]. \quad (1)$$

Here, the first term describes an independent oscillator using the second-quantization operators, and Φ is the interaction between the two engine components, where $\hat{x}$ is the position operator of the oscillator, and $y(\tau)$ is the piston coordinate. In addition to using $\hbar\Omega$ as the energy scale, it is convenient to express lengths in terms of the quantum oscillator length and time in terms of the oscillator periods so that $t = 2\pi\tau/\Omega$.

For this paper, the interaction is set to

$$\Phi[\hat{x}, y(\tau)] = \Phi_0 \exp\left[-\frac{\hat{x}^2 + y^2(\tau)}{2\sigma^2}\right]. \quad (2)$$

There are two reasons for choosing this form of Φ. First, the amplitude and the extent of the Gaussian are easily tunable, making this type of interaction very convenient for illustrating the relevant behavior. Second, y and $\hat{x}$ are separable, simplifying the computational procedure. With this choice, the matrix elements of $\hat{H}(\tau)$ in the Fock space become

$$\langle j|\hat{H}(\tau)|k\rangle = \left(j + \frac{1}{2}\right)\delta_{j,k} + \Phi_0\, e^{-[y^2(\tau)]/(2\sigma^2)} \times \langle j| \exp\left(-\frac{\hat{x}^2}{2\sigma^2}\right)|k\rangle. \quad (3)$$

The form of Eq. (3) indicates that the interaction matrix must be computed only once for a particular choice of σ and scaled based on $y(\tau)$ as the piston moves, substantially speeding up numerical calculations. Although $\langle j| \exp(-\hat{x}^2/2\sigma^2)|k\rangle$ can be computed analytically for the quantum oscillator wave functions, producing Gaussian hypergeometric functions, the integrals in the simulations are taken using Gaussian quadratures to avoid potential issues associated with the numerical implementation of these special functions.

A key ingredient in the engine operation is the temperature-dependent interaction between the working fluid and the piston. To illustrate this effect, let the oscillator-piston system be in a thermal state, described by the density operator $\hat{\rho}(\omega_T, \hat{H}) = \exp(-\hat{H}/\omega_T)/\mathrm{tr}[\exp(-\hat{H}/\omega_T)]$, where $\omega_T = k_B T/\hbar\Omega$ is the thermal frequency corresponding to temperature T, k_B is the Boltzmann constant, and $\hat{H}$ is given by Eq. (1). The interaction energy is computed from $\mathrm{tr}(\hat{\Phi}\hat{\rho})$ with $\hat{\Phi}$ matrix elements given by the second term in Eq. (3). Setting $\Phi_0 = -5$, the value that will be used in subsequent simulations, the energy is calculated as a function of ω_T and y for several values of σ with the results given in Fig. 2. As expected, the energy of the system is the lowest for a wide interaction term (large σ) when the piston is close to the oscillator and the temperature is low. Increasing either ω_T or y reduces the magnitude of the interaction.

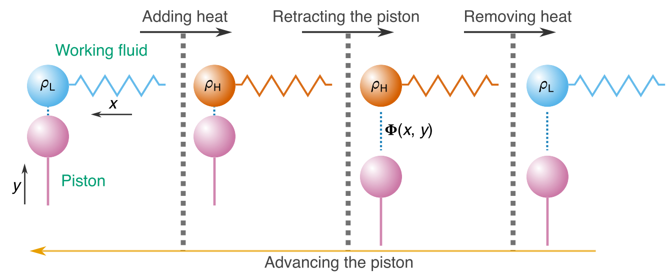

FIG. 1. *Engine cycle schematic.* The four phases of the engine cycle proceed in the direction indicated by the arrows. The working fluid is a quantum harmonic oscillator. It is coupled to an externally controlled piston via an attractive interaction, so adding heat to the working fluid reduces the coupling strength. Conversely, cooling the oscillator makes the interaction stronger. The power stroke of the cycle occurs when the piston is advanced, as denoted by the orange arrow.

At each of the four phases of the proposed cycle, the corresponding system energies are given by

$$\begin{aligned}
E_\mathrm{A}^\mathrm{hot} &= \mathrm{tr}\left[\hat{H}_\mathrm{A}\hat{\rho}\left(\omega_T^\mathrm{hot}, \hat{H}_\mathrm{A}\right)\right], \\
E_\mathrm{R}^\mathrm{hot} &= \mathrm{tr}\left[\hat{H}_\mathrm{R}\hat{\mathcal{U}}\hat{\rho}\left(\omega_T^\mathrm{hot}, \hat{H}_\mathrm{A}\right)\hat{\mathcal{U}}^\dagger\right], \\
E_\mathrm{R}^\mathrm{cold} &= \mathrm{tr}\left[\hat{H}_\mathrm{R}\hat{\rho}\left(\omega_T^\mathrm{cold}, \hat{H}_\mathrm{R}\right)\right], \\
E_\mathrm{A}^\mathrm{cold} &= \mathrm{tr}\left[\hat{H}_\mathrm{A}\hat{\mathcal{U}}^\dagger\hat{\rho}\left(\omega_T^\mathrm{cold}, \hat{H}_\mathrm{R}\right)\hat{\mathcal{U}}\right],
\end{aligned} \quad (4)$$

in this order. The subscripts R and A denote the position of the piston as retracted and advanced. The superscripts hot and cold indicate whether the last bath that the system contacted was hot or cold. The unitary operator $\hat{\mathcal{U}}$ describes the evolution of the system during the piston retraction. For simplicity, the piston is assumed to move at a constant speed so that $y(\tau) = y_\mathrm{init} + \tau(y_\mathrm{final} - y_\mathrm{init})/\tau_p$ for $0 \leqslant \tau \leqslant \tau_p$, where τ_p is the duration of the retraction and advancing phases. For finite τ_p, $\hat{\mathcal{U}}$ can be computed numerically from

$$\frac{d}{d\tau}\hat{\mathcal{U}}(\tau, \tau') = -2\pi i \hat{H}(\tau)\hat{\mathcal{U}}(\tau, \tau'), \quad (5)$$

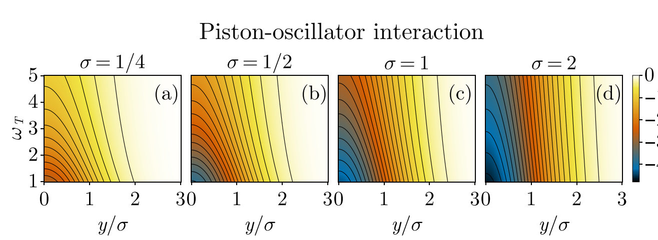

FIG. 2. *Controlling the interaction.* Dependence of the interaction energy on temperature and piston position for $\Phi_0 = -5$ and several values of σ. The black lines are energy equicontours separated by 0.2. Retracting the piston or raising the oscillator temperature reduces the interaction strength.

where the factor of 2π originates from the definition of τ. In the next section, the fifth-order Runge-Kutta method with $\hat{\mathcal{U}}(\tau', \tau') = 1$ is used to obtain this operator. First, however, it is instructive to explore the efficiency of the cycle in the adiabatic limit.

B. Efficiency

Adiabatic piston motion means that the matrix corresponding to the density operator remains fixed in the instantaneous basis as the Hamiltonian is varied. Thus, if ρ_{hot} is the matrix representation of $\hat{\rho}(\omega_T^{\text{hot}}, \hat{H}_{\text{A}})$ computed in the basis of eigenstates of $\hat{H}_{\text{A}}$, the post-retraction state $\hat{\mathcal{U}}\hat{\rho}(\omega_T^{\text{hot}}, \hat{H}_{\text{A}})\hat{\mathcal{U}}^\dagger$ computed in the basis of eigenstates of $\hat{H}_{\text{R}}$ will also be ρ_{hot}. Similarly, $\hat{\rho}(\omega_T^{\text{cold}}, \hat{H}_{\text{R}})$ and $\hat{\mathcal{U}}^\dagger\hat{\rho}(\omega_T^{\text{cold}}, \hat{H}_{\text{R}})\hat{\mathcal{U}}$ will also take the same form ρ_{cold} but correspond to two different bases.

The cycle efficiency $\eta = W/Q_{\text{in}}$ in the adiabatic regime is given by

$$\eta = \frac{\text{tr}\big[(\rho_{\text{hot}} - \rho_{\text{cold}})\big(\hat{H}_{\text{A}}^D - \hat{H}_{\text{R}}^D\big)\big]}{\text{tr}\big[(\rho_{\text{hot}} - \rho_{\text{cold}})\hat{H}_{\text{A}}^D\big]} = 1 - \frac{\text{tr}\big[(\rho_{\text{hot}} - \rho_{\text{cold}})\hat{H}_{\text{R}}^D\big]}{\text{tr}\big[(\rho_{\text{hot}} - \rho_{\text{cold}})\hat{H}_{\text{A}}^D\big]}, \tag{6}$$

where $W = E_{\text{A}}^{\text{hot}} - E_{\text{R}}^{\text{hot}} + E_{\text{R}}^{\text{cold}} - E_{\text{A}}^{\text{cold}} > 0$ and $Q_{\text{in}} = E_{\text{A}}^{\text{hot}} - E_{\text{A}}^{\text{cold}} > 0$ correspond to the work performed and the heat input, respectively. The superscript D indicates that the Hamiltonian matrices are diagonal.

The efficiency of the adiabatic cycle is bounded by the Carnot limit. Specifically, when $\omega_T^{\text{cold}} \to 0$, the Carnot efficiency approaches 1. In the present case,

$$\eta \to 1 - \frac{\text{tr}\big[\rho_{\text{hot}}\hat{H}_{\text{R}}^D\big] - E_{\text{R}}^0}{\text{tr}\big[\rho_{\text{hot}}\hat{H}_{\text{A}}^D\big] - E_{\text{A}}^0} < 1, \tag{7}$$

where $E_{\text{A/R}}^0$ are the ground state energies of the working fluid when the piston is in the advanced/retracted position. Hence, the efficiency of this cycle is strictly below the Carnot efficiency in the $\omega_T^{\text{cold}} \to 0$ limit. Raising ω_T^{cold} decreases the denominator and numerator as the heat flow between the working fluid and the baths diminishes. Crucially, the denominator decreases faster because $\text{tr}[\rho_{\text{cold}}(\hat{H}_{\text{R}}^D - \hat{H}_{\text{A}}^D)] > 0$ for an attractive piston-oscillator interaction. As a result, the efficiency decreased monotonically with increasing ω_T^{cold}.

Raising ω_T^{hot} does not take η to 1, as happens in Carnot engines with $\omega_T^{\text{hot}} \to \infty$. The reason for this behavior is the fact that $\hat{\Phi}$ affects lower working fluid states more by design. Thus, if the temperature of the hot bath gets sufficiently high, $E_{\text{A}}^{\text{hot}}$ and $E_{\text{R}}^{\text{hot}}$ tend to ω_T^{hot} as the interaction portion becomes irrelevant. Thus, in the $\omega_T^{\text{hot}} \to \infty$ limit, the fraction in Eq. (6) tends to 1, setting η to zero.

As can be seen from the analysis, unlike certain other quantum engines, the cycle proposed here does not make it possible to surpass the Carnot limit in the adiabatic regime. Nevertheless, future research could explore variations of this engine to potentially overcome the Carnot efficiency.

C. Nonadiabatic effects

If the time of piston movement τ_p is finite, as it will be during engine operation, the evolution of the system is no longer guaranteed to be adiabatic. Therefore, it is useful to explore how slowly the piston has to move for the nonadiabatic effects to be negligible using the following procedure.

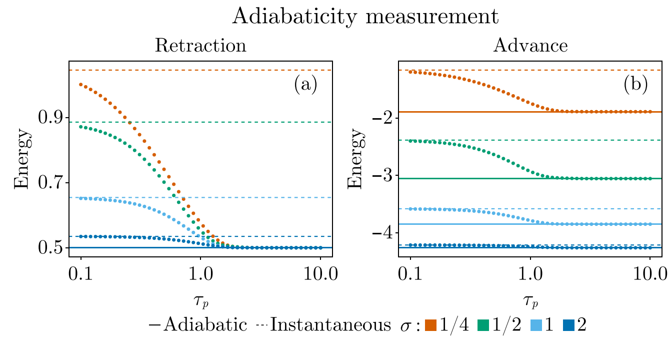

FIG. 3. *Role of finite* τ_p. System energy as a function of time of piston retraction and advance τ_p for $\Phi_0 = -5$ and several values of σ. The piston moves between $y = 0$ and $y = 10\sigma$. The numerically computed results for finite τ_p are bounded by the adiabatic ($\tau_p \to \infty$) and instantaneous ($\tau_p \to 0$) results. Smaller σ leads to greater nonadiabatic effects.

Starting with the Hamiltonians corresponding to retracted ($y = 10\sigma$) and advanced ($y = 0$) pistons, one determines their ground states $|R\rangle$ and $|A\rangle$, respectively. If the piston were retracted (advanced) adiabatically, the energy of the system would end up as $\langle R|\hat{H}_{\text{R}}|R\rangle$ ($\langle A|\hat{H}_{\text{A}}|A\rangle$) because the system would remain in its ground state. Conversely, for an instantaneous change of piston position, the state would not have time to evolve, and the final energy would be $\langle A|\hat{H}_{\text{R}}|A\rangle$ ($\langle R|\hat{H}_{\text{A}}|R\rangle$). Hence, the actual final energy is bounded by these two values.

To obtain the system energy for a finite piston movement time τ_p, one uses the fact that the state evolves following the time-dependent Schrödinger equation:

$$\frac{d}{d\tau}|\Psi(\tau)\rangle = -2\pi i\hat{H}(\tau)|\Psi(\tau)\rangle. \tag{8}$$

Solving Eq. (8) using the fifth-order Runge-Kutta method starting with $|\Psi(0)\rangle = |A\rangle$ and $|\Psi(0)\rangle = |R\rangle$, the final energy can be computed as a function of τ_p for a constant-speed piston with the results given in Fig. 3. As expected, the finite-τ_p energies lie between the adiabatic and instantaneous results for both retraction and advance of the piston. Figure 3 suggests that $\tau_p \gtrapprox 5$ is sufficiently slow to avoid the nonadiabatic effects associated with the piston movement even for small values of σ considered here. However, care should be taken because, even at $\tau_p = 5$, one can observe an energy creep after a sufficient number of engine cycles, as shown below.

III. ENGINE OPERATION

A. Simulation protocol

Conceptually, the most straightforward way to heat up or cool down the working fluid is to connect it to a bath. For the sake of illustration, modeled in this paper are the baths using single-oscillator modes described by a density operator corresponding to a thermal state, as was done in Ref. [18]. The bath contact is described using the collision model [38]: every time the working fluid is connected to a bath, the latter is reset to the appropriate thermal state $\hat{\rho}_b =$

$\exp(-b^\dagger b/\omega_T)/\mathrm{tr}[\exp(-b^\dagger b/\omega_T)]$. Naturally, the single-bath modes do not operate as true thermal reservoirs and do not bring the working fluid to a thermal state with the bath temperature [18]. They can, instead, be regarded as ancillae that deliver energy to or extract it from the working fluid, functioning as energy bridges. While a bath mode is disconnected from the engine, it can be returned to its precontact state using optical means (like laser cooling) or coupling it to a true thermodynamic reservoir at the desired temperature.

To streamline the discussion, the frequency of the bath oscillators is taken to be identical to that of the working fluid. In addition to eliminating a parameter, setting the oscillator frequencies to the same value facilitates the energy exchange between the modes. There are various ways of coupling the baths to the engine, with the simplest being a linear interaction $a^\dagger b + b^\dagger a$. Here, however, assume that the coupling between the oscillators decreases with their separation and use a Gaussian term, just as the piston interaction, given by

$$Y(\hat{x}, \hat{z}) = Y_0 \exp\left[-\frac{(\hat{x}-x_0)^2 + (\hat{z}-z_0)^2}{2\lambda^2}\right], \tag{9}$$

where $\hat{z}$ is the position of the bath oscillator. The offsets x_0 and z_0 mean that the equilibrium points of the two oscillators do not coincide in the xz plane and are introduced to allow modes with different parities to couple, which would be forbidden by a symmetric potential $\exp(-\hat{x}^2/2\lambda^2)$. Setting $x_0 = z_0 = \lambda = 1$ and using the separability of the interaction term, one can write the full interaction matrix $Y = Y_0 Y_{\mathrm{single}} \otimes Y_{\mathrm{single}}$, where Y_{single} elements are given with elements $\langle j|\exp[-(x-x_0)^2/2\lambda^2]|k\rangle$ for all the Fock states in the single-oscillator basis. Like the matrix elements in Eq. (3), these are computed using Gaussian quadratures.

The motivation behind using the Gaussian form instead of the linear coupling has to do with the envisioned implementation of the engine. A possible setup would use either a gas of cold atoms in an optical trap or a particle held by optical tweezers as the working fluid and bath oscillators. It is then reasonable to assume that the interaction should decrease with the separation of the oscillator masses, and a Gaussian term is a particularly easy form to be used for illustration.

For simplicity, the interaction between the bath and the working fluid is assumed to be switched on and off instantaneously so that, when the piston is stationary, the Hamiltonian is time independent, leading to

$$\begin{aligned}\hat{H}_{\mathrm{bath}} = &\left[\left(\hat{a}^\dagger\hat{a} + \tfrac{1}{2}\right) + \Phi(\hat{x}, y)\right] \otimes \mathbf{1}\\ &+ \mathbf{1} \otimes \left(\hat{b}^\dagger\hat{b} + \tfrac{1}{2}\right) + Y_0 Y_{\mathrm{single}} \otimes Y_{\mathrm{single}},\end{aligned} \tag{10}$$

where $\mathbf{1}$ is the identity. The corresponding time evolution operator $\hat{\mathcal{B}} = \exp(-2\pi i \tau_b \hat{H}_{\mathrm{bath}})$, where τ_b is the contact time between the fluid and the bath, taken to be the same for both hot and cold baths.

To demonstrate the engine operation, the piston motion and bath contact are taken to have the same duration τ_p. Two different σ's ($\frac{1}{2}$ and 2) and τ_p's (5 and 10) are used for a total of four configurations. The bath temperatures are set to $\omega_T^{\mathrm{cold}} = \frac{1}{10}$ and $\omega_T^{\mathrm{hot}} = 5$, and the Fock basis for each oscillator contains 51 states. For each configuration, the working fluid is initialized in the thermal state at ω_T^{cold} with the piston in the advanced position. It is then taken 80 times through the cycle described by Eq. (11). As will be shown, the system reaches a steady state in $\ll$80 cycles. The reason for the extended simulation is to demonstrate the long-term stability and to show the parasitic effect that can arise due to weak but nonzero nonadiabatic effects, as mentioned at the end of Sec. II C. At the end of each stroke, the energy of the working fluid is computed by taking the trace of the product of its density operator with $(\hat{a}^\dagger\hat{a} + \frac{1}{2}) + \Phi(\hat{x}, y)$ for the appropriate value of y.

B. Bath-powered setup

Following Fig. 1, the cycle begins with heat addition. Thus, if the state of the working fluid in the beginning of the nth cycle is given by $\hat{\rho}_n$, the state of the fluid in the beginning of the following cycle is

$$\hat{\rho}_{n+1} = \hat{\mathcal{U}}^\dagger \mathrm{tr}_b[\hat{\mathcal{B}}\{\hat{\mathcal{U}}\mathrm{tr}_b[\hat{\mathcal{B}}(\hat{\rho}_n \otimes \hat{\rho}_h)\hat{\mathcal{B}}^\dagger]\hat{\mathcal{U}}^\dagger \otimes \hat{\rho}_c\}\hat{\mathcal{B}}^\dagger]\hat{\mathcal{U}}, \tag{11}$$

where $\hat{\mathcal{U}}$ corresponds to the operator describing the piston retraction. Equation (11) should be read from the inside outward to follow the cycle. First, the fluid is coupled to the hot bath in thermal state $\hat{\rho}_h$, as shown by the tensor product. After that, the composite system is allowed to evolve in time by applying operators $\hat{\mathcal{B}}$ and $\hat{\mathcal{B}}^\dagger$. To decouple the working fluid from the bath, a partial trace tr_b is performed with respect to the bath. Next, the piston is retracted by sandwiching the fluid state between $\hat{\mathcal{U}}$ and $\hat{\mathcal{U}}^\dagger$. Then the fluid is coupled to a cold bath $\hat{\rho}_c$, and the two-oscillator system is evolved using the same operator $\hat{\mathcal{B}}$ as was used for the hot bath, followed by a decoupling. Finally, the piston is advanced, as can be seen from the reversed application of $\hat{\mathcal{U}}^\dagger$ and $\hat{\mathcal{U}}$, completing the cycle. Thus, instead of evolving the state every time the piston moves, one needs to compute $\hat{\mathcal{U}}$ only once, making a multicycle calculation more efficient.

The results of the simulation are given in Fig. 4 with the system energies at the end of each stroke shown in panels (a)–(d). The x coordinate labels the cycle and, for each cycle, the order of the points is advanced cold $\rightarrow$ advanced hot $\rightarrow$ retracted hot $\rightarrow$ retracted cold, after which one moves to advanced cold of the next cycle. Figures 4(a)–4(d) demonstrate that even the single-oscillator bath, where the working fluid does not actually reach a thermal state, is sufficient for the engine to output work as it reaches a steady state. This fact is encouraging from the experimental point of view because even the imperfect thermalization is acceptable, making the requirement on the experimental realization of the cycle less stringent. One can see that the faster cycle shows a small creep in energy, more substantial for $\sigma = \frac{1}{2}$. This creep can be attributed to the nonadiabatic effects of the piston movement: According to Fig. 3, smaller σ's are more susceptible to this effect.

Figure 4(e) plots the cycle-resolved efficiency for each setup, shown to also reach a steady state. Efficiency for the adiabatic cycle obtained from Eq. (6), where $\rho_{\mathrm{H/C}}$ are taken to be thermal states with $\omega_T^{\mathrm{hot/cold}}$, is plotted along with the simulation results. Because the cycle operation is not adiabatic and the working fluid does not thermalize during its contact with the baths, the efficiencies differ. This, however, does not present a problem from the experimental perspective, as discussed above.

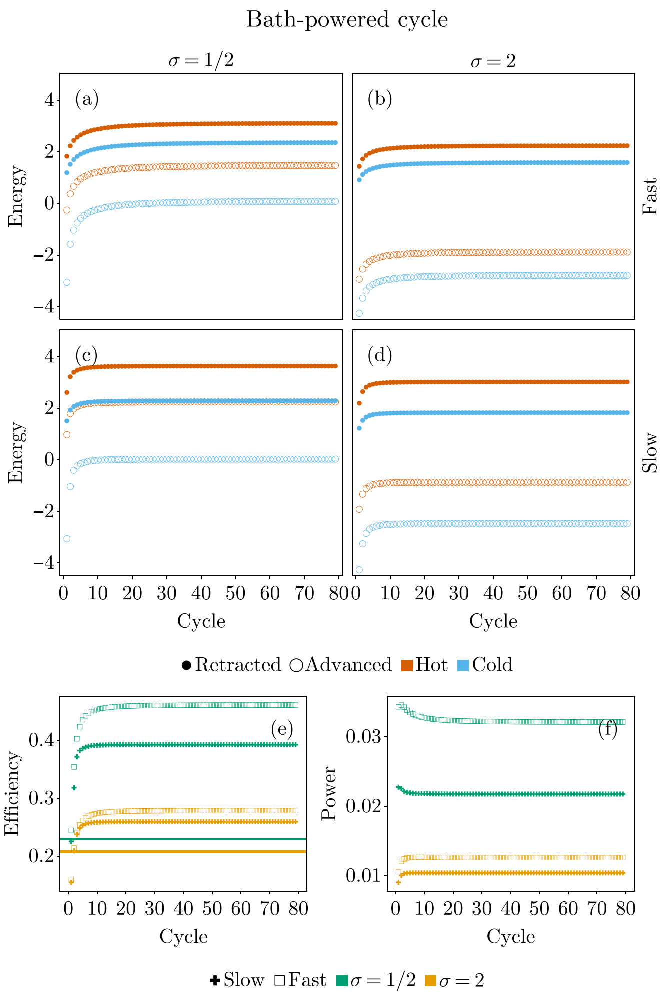

FIG. 4. *Bath engine operation*. 80 cycles of a bath-powered engine initialized in a thermal state and evolved using Eq. (11) with $\omega_T^{\text{hot}} = 5$ and $\omega_T^{\text{cold}} = \frac{1}{10}$. The interaction between the baths and the gas is given by Eq. (9) with $Y_0 = x_0 = z_0 = 1$. The baths and the oscillator Fock spaces contain 51 states. The piston interaction is given by Eq. (2) with $\Phi_0 = -5$. (a)–(d) System energy at each phase of the cycle as a function of cycle number. For the fast engine (top row), the time of each stroke is 5, while for the slow one (bottom row), it is 10. (e) Efficiency for each of the engines as a function of the cycle number, computed by dividing the total work output by heat input. (f) The power of the engines, obtained by dividing the total work output by the duration of a cycle.

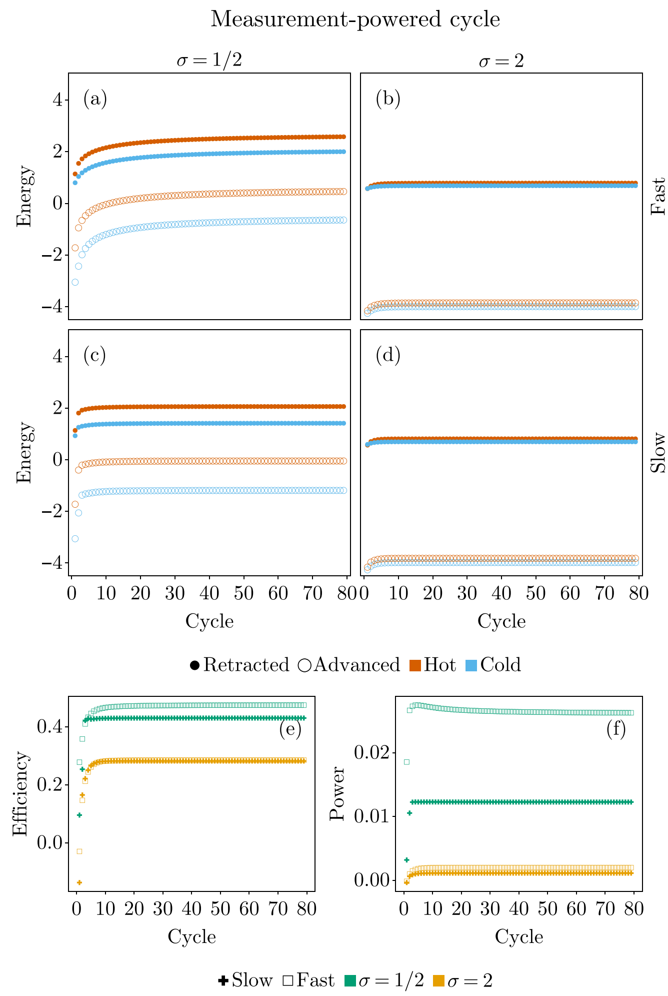

FIG. 5. *Measurement engine operation*. 80 cycles of a measurement-powered engine initialized in a thermal state and evolved using Eq. (12) with $\omega_T^{\text{cold}} = \frac{1}{10}$. The interaction between the baths and the gas is given by Eq. (9) with $Y_0 = x_0 = z_0 = 1$. The baths and the oscillator Fock spaces contain 51 states. The piston interaction is given by Eq. (2) with $\Phi_0 = -5$. (a)–(d) System energy at each phase of the cycle as a function of cycle number. For the fast engine (top row), the time of each stroke is 5, while for the slow one (bottom row), it is 10. (e) Efficiency for each of the engines as a function of the cycle number, computed by dividing the total work output by heat input. (f) The power of the engines, obtained by dividing the total work output by the duration of a cycle.

Curiously, the efficiency of the fast cycles is higher than the slow ones. This efficiency gain, however, comes at the expense of the work performed. Figure 4(f) provides the cycle-resolved power for each engine configuration obtained by dividing the net work output by $4\tau_p$. Even though the fast cycle takes half the time compared with the slow one, its power is not doubled, indicating that the slow cycle delivers more work. One can confirm this statement by comparing the separation between red markers for each cycle with that of the blue markers. The former corresponds to the work done on the engine, while the latter is the work done by the engine. The greater the difference, the more net work the engine outputs. It is evident that the difference is larger for the slow cycles for both σ's.

C. Measurement-powered setup

Changing to the power source from a hot bath to measurements while keeping everything else the same amounts to replacing $\text{tr}_b[\hat{\mathcal{B}}(\hat{\rho}_n \otimes \hat{\rho}_h)\hat{\mathcal{B}}^\dagger] \to \text{diag}(\hat{\rho}_n)$ in Eq. (11), corresponding to the measurement. Here, $\text{diag}(\hat{\rho}_n)$ means that the off-diagonal elements (coherence terms) are set to zero, giving a classical probability. Hence, the cycle expression becomes

$$\hat{\rho}_{n+1} = \hat{\mathcal{U}}^\dagger \text{tr}_b\{\hat{\mathcal{B}}[\hat{\mathcal{U}}\,\text{diag}(\hat{\rho}_n)\hat{\mathcal{U}}^\dagger \otimes \hat{\rho}_c]\hat{\mathcal{B}}^\dagger\}\hat{\mathcal{U}}. \qquad (12)$$

The results for a set of four simulations using the same two values of σ and phase duration as above are given in Fig. 5. While the $\sigma = \frac{1}{2}$ setup looks qualitatively similar to the corresponding configurations in Fig. 4, including the energy creep in the fast cycle, $\sigma = 2$ is drastically different, showing virtually no work output. This outcome is attributable to the fact that the piston-generated potential is wide on the scale of the wave functions of the oscillator, resulting in a very weak harmonic mixing. Therefore, the measurement does not result in a substantial transfer of energy to the oscillator since the oscillator does not transition to higher energy states.

The efficiency for the measurement-powered cycle is similar to the bath-powered one, as seen by comparing Figs. 4(e) and 5(e). To compute the power, the net work output is divided by $3\tau_p$ since the measurement is assumed to be much faster than τ_p. The power for $\sigma = \frac{1}{2}$ is comparable with the bath-powered setup. In the $\sigma = 2$ case, on the other hand, the vanishing work output results in negligible power.

The key takeaway of this section is that, despite the restricted and artificial form of the baths, the engine reaches a steady state and can output useful work. Enhancing the ability of the oscillator to expel the waste heat by using a real reservoir and optimizing the piston and bath interaction profiles will improve the work output.

IV. SUMMARY

In this paper, a realization of a single-piston quantum engine has been introduced and simulated, where the role of the working fluid is played by a harmonic oscillator. By taking advantage of the fact that the interaction between the working fluid and the piston can be controlled by modifying the energy of the oscillator, it has been shown that, by following a cycle comprised of heating/cooling of the oscillator and piston motion toward and away from the oscillator, the engine can output work. Two general protocols of engine fueling have been discussed: bath and measurement powered, with both successfully demonstrating stable work output over multiple cycles, indicating a steady state of operation. For simplicity, the heat reservoirs used here comprised single thermal harmonic oscillator modes. Even though these modes do not function as true thermodynamic baths, the fact that the engine produces work suggests that the engine operation scheme is robust.

It is possible to realize the proposed cycle using existing techniques. For the bath-powered setup, one can employ the scheme given in Ref. [39]. In this setup, a single ultracold atom in an optical trap plays the role of the working fluid, while a cloud of atoms of different species in the trap acts as a bath. An external magnetic field is used to control the interaction between the working fluid and the bath through Feshbach resonances. Reference [39] uses species-specific optical tweezers to control the confinement of the working fluid, demonstrating quantum Otto, Diesel, and Carnot cycles. For the cycle proposed in this paper, the confining potential of the working fluid remains fixed, and the role of a piston can be played by another atom or a nanoparticle held in optical tweezers which can be moved with respect to the optical trap containing the bath and the working-fluid atom. The temperature of the bath can be lowered by laser cooling and raised by either driving or connecting the bath cloud to a larger external reservoir, so that the bath functions as an ancilla, as was described in the text. Alternatively, the energy of the bath can also be modified by varying its confinement [39]. Finally, one could use the cloud only as a hot bath and cool the working fluid using Raman sideband cooling [40].

For projective measurements, one could employ the protocol described in Ref. [41]. In this approach, the energy of the oscillator is lowered until it reaches the ground state. The number of lowering operations n is recorded and the oscillator is then brought to the nth excited level by performing n raising operations. A possible difficulty here is that, during the measurement, the oscillator remains in contact with the piston. Consequently, performing n raising operations is not guaranteed to bring it to the nth excited state, as the final state will depend on the time scale difference between the raising procedure and eigenstate hybridization due to the piston potential. A simplified setup could replace the oscillator by a two-state system which interacts differently with the piston. In this case, one would, at most, need to perform a single raising operation, thereby reducing the amount of time required for this procedure.

ACKNOWLEDGMENTS

The author acknowledges the National Research Foundation, Prime Minister Office, Singapore, under its Medium Sized Centre Programme and the support by Yale-NUS College (through a Start-up Grant).

[1] S. Bhattacharjee and A. Dutta, Quantum thermal machines and batteries, Eur. Phys. J. B **94**, 239 (2021).

[2] N. M. Myers, O. Abah, and S. Deffner, Quantum thermodynamic devices: From theoretical proposals to experimental reality, AVS Quantum Sci. **4**, 027101 (2022).

[3] X. L. Huang, T. Wang, and X. X. Yi, Effects of reservoir squeezing on quantum systems and work extraction, Phys. Rev. E **86**, 051105 (2012).

[4] S. Chand and A. Biswas, Single-ion quantum Otto engine with always-on bath interaction, Europhys. Lett. **118**, 60003 (2017).

[5] G. Thomas, N. Siddharth, S. Banerjee, and S. Ghosh, Thermodynamics of non-Markovian reservoirs and heat engines, Phys. Rev. E **97**, 062108 (2018).

[6] S. Chand, S. Dasgupta, and A. Biswas, Finite-time performance of a single-ion quantum Otto engine, Phys. Rev. E **103**, 032144 (2021).

[7] A. D. Campo, J. Goold, and M. Paternostro, More bang for your buck: Super-adiabatic quantum engines, Sci. Rep. **4**, 6208 (2014).

[8] J. Roßnagel, O. Abah, F. Schmidt-Kaler, K. Singer, and E. Lutz, Nanoscale heat engine beyond the carnot limit, Phys. Rev. Lett. **112**, 030602 (2014).

[9] R. Kosloff and Y. Rezek, The quantum harmonic Otto cycle, Entropy **19**, 136 (2017).

[10] B. Reid, S. Pigeon, M. Antezza, and G. D. Chiara, A self-contained quantum harmonic engine, Europhys. Lett. **120**, 60006 (2017).

[11] P. Chattopadhyay, Non-commutative space: Boon or bane for quantum engines and refrigerators, Eur. Phys. J. Plus **135**, 302 (2020).

[12] P. Chattopadhyay, T. Pandit, A. Mitra, and G. Paul, Quantum cycle in relativistic non-commutative space with

generalized uncertainty principle correction, Physica A **584**, 126365 (2021).

[13] T. Pandit, P. Chattopadhyay, and G. Paul, Non-commutative space engine: A boost to thermodynamic processes, Mod. Phys. Lett. A **36**, 2150174 (2021).

[14] F. Cavaliere, M. Carrega, G. De Filippis, V. Cataudella, G. Benenti, and M. Sassetti, Dynamical heat engines with non-Markovian reservoirs, Phys. Rev. Res. **4**, 033233 (2022).

[15] Z. Fei, J. F. Chen, and Y. H. Ma, Efficiency statistics of a quantum Otto cycle, Phys. Rev. A **105**, 022609 (2022).

[16] F. Cavaliere, L. Razzoli, M. Carrega, G. Benenti, and M. Sassetti, Hybrid quantum thermal machines with dynamical couplings, iScience **26**, 106235 (2023).

[17] J. F. Santos and P. Chattopadhyay, $\mathcal{PT}$-symmetry effects in measurement-based quantum thermal machines, Physica A **632**, 129342 (2023).

[18] A. Rodin, Three-dimensional harmonic oscillator as a quantum Otto engine, Phys. Rev. Res. **6**, 013180 (2024).

[19] M. Boubakour, T. Fogarty, and T. Busch, Interaction-enhanced quantum heat engine, Phys. Rev. Res. **5**, 013088 (2023).

[20] M. Carrega, L. Razzoli, P. A. Erdman, F. Cavaliere, G. Benenti, and M. Sassetti, Dissipation-induced cooperative advantage in a quantum thermal machine, AVS Quantum Science **6**, 025001 (2024).

[21] K. Zhang, F. Bariani, and P. Meystre, Quantum optomechanical heat engine, Phys. Rev. Lett. **112**, 150602 (2014).

[22] Á. Tejero, D. Manzano, and P. I. Hurtado, Atom-doped photon engine: Extracting mechanical work from a quantum system via radiation pressure, Phys. Rev. E **109**, 024141 (2024).

[23] S. Chand and A. Biswas, Measurement-induced operation of two-ion quantum heat machines, Phys. Rev. E **95**, 032111 (2017).

[24] C. Elouard, D. Herrera-Martí, B. Huard, and A. Auffèves, Extracting work from quantum measurement in maxwell's demon engines, Phys. Rev. Lett. **118**, 260603 (2017).

[25] C. Elouard, D. A. Herrera-Martí, M. Clusel, and A. Auffèves, The role of quantum measurement in stochastic thermodynamics, npj Quantum Inf. **3**, 9 (2017).

[26] S. Chand and A. Biswas, Critical-point behavior of a measurement-based quantum heat engine, Phys. Rev. E **98**, 052147 (2018).

[27] C. Elouard and A. N. Jordan, Efficient quantum measurement engines, Phys. Rev. Lett. **120**, 260601 (2018).

[28] A. Das and S. Ghosh, Measurement based quantum heat engine with coupled working medium, Entropy **21**, 1131 (2019).

[29] L. Bresque, P. A. Camati, S. Rogers, K. Murch, A. N. Jordan, and A. Auffèves, Two-qubit engine fueled by entanglement and local measurements, Phys. Rev. Lett. **126**, 120605 (2021).

[30] S. K. Manikandan, C. Elouard, K. W. Murch, A. Auffèves, and A. N. Jordan, Efficiently fueling a quantum engine with incompatible measurements, Phys. Rev. E **105**, 044137 (2022).

[31] M. S. Alam and B. P. Venkatesh, Two-stroke quantum measurement heat engine, arXiv:2201.06303.

[32] É. Jussiau, L. Bresque, A. Auffèves, K. W. Murch, and A. N. Jordan, Many-body quantum vacuum fluctuation engines, Phys. Rev. Res. **5**, 033122 (2023).

[33] A. Rodin, Advantages of non-Hookean coupling in a measurement-fueled two-oscillator engine, arXiv:2311.04446.

[34] J. Bezanson, A. Edelman, S. Karpinski, and V. B. Shah, Julia: A fresh approach to numerical computing, SIAM Rev. **59**, 65 (2017).

[35] S. Danisch and J. Krumbiegel, Makie.jl: Flexible high-performance data visualization for Julia, J. Open Source Softw. **6**, 3349 (2021).

[36] B. Wong, Color blindness, Nat. Methods **8**, 441 (2011).

[37] https://github.com/rodin-physics/quantum-oscillator-engine.

[38] F. Ciccarello, S. Lorenzo, V. Giovannetti, and G. M. Palma, Quantum collision models: Open system dynamics from repeated interactions, Phys. Rep. **954**, 1 (2022).

[39] G. Barontini and M. Paternostro, Ultra-cold single-atom quantum heat engines, New J. Phys. **21**, 063019 (2019).

[40] A. M. Kaufman, B. J. Lester, and C. A. Regal, Cooling a single atom in an optical tweezer to its quantum ground state, Phys. Rev. X **2**, 041014 (2012).

[41] S. An, J. N. Zhang, M. Um, D. Lv, Y. Lu, J. Zhang, Z. Q. Yin, H. T. Quan, and K. Kim, Experimental test of the quantum Jarzynski equality with a trapped-ion system, Nat. Phys. **11**, 193 (2015).